X-ray imaging with amorphous selenium: Theoretical feasibility of the liquid crystal light valve for radiography

Pia-Krista Rieppo and J. A. Rowlands[a)]
Departments of Medical Biophysics and Medical Imaging, University of Toronto, Research Building, Sunnybrook Health Science Centre, 2075 Bayview Avenue, North York, Ontario, M4N 3M5 Canada

(Received 1 November 1996; accepted for publication 30 April 1997)

A novel radiographic imaging system based on a liquid crystal light valve is described. A liquid crystal light valve is a photon addressed spatial light modulator that consists of a high resolution, solid-state electrostatic detector (photoconductor) and an electro-optic light modulator (liquid crystal cell) physically coupled in a sandwich structure. We propose a light valve with a thick, x-ray sensitive photoconductive layer and call the system under study the x-ray light valve (XLV). The image formation in the XLV is based on x-ray exposure controlled modulation of light from an external source; the XLV is essentially an x-ray image intensifier that allows the image brightness to be adjusted independently from the x-ray exposure. Thus the XLV may be coupled to an optical imager, such as a charge coupled device (CCD), for image digitization without a secondary quantum sink. A model of the XLV operation is developed to investigate its sensitivity, speed, noise, and resolution. The imaging properties of the XLV are found to be time dependent, which leads to an unusual transmission versus exposure characteristic. The feasibility of clinical use of the XLV based on amorphous selenium (*a*-Se) photoconductor and a twisted nematic liquid crystal cell is analyzed, and the device is shown to be adaptable to a variety of radiographic imaging tasks. [S0094-2405(97)00508-7]

Key words: digital imaging, image intensifier, light valve, photoconductor, selenium, radiographic system, spatial light modulator

I. INTRODUCTION

Currently most radiographic imaging systems in clinical use are based on a light emitting x-ray detector—a phosphor screen. The resulting optical image is conventionally used to expose a photographic film. However, in recent years there has been increasing interest in digital alternatives to film-screen radiography. Digital imaging would potentially allow improved image quality via independent optimization of the detector and the display as well as image processing, electronic transfer and storage of image data, and computer aided diagnosis.

Many of the proposed digital systems also rely on the use of a phosphor screen and thus require conversion of light to an electronic signal.[1–3] In such conversion there will be some signal loss due to inefficiencies in coupling between the screen and the later stage components. For example, demagnification via optics is required if a large area phosphor screen is coupled to an optical imager such as a charge coupled device (CCD). For the large demagnification required in most clinical situations, the coupling efficiency is so poor that few light photons reach the optical detector and are converted to electrons.[2,4] When only a few electrons represent an x ray, a secondary quantum sink may be present whereby the x-ray quantum noise no longer is the dominant source of noise in the image; this can degrade the image signal-to-noise ratio (SNR).[5] In medical imaging, where x-ray exposure must be minimized to reduce risk to the patient, significant extra noise due to a secondary quantum sink is unacceptable.

This paper addresses a novel radiographic system that incorporates the x-ray absorption, image formation, and amplification stages within a simple, flat panel structure, and potentially eliminates problems related to a secondary quantum sink. The system, to be called the x-ray light valve (XLV), is based on liquid crystal light valves used as optically addressed spatial light modulators[6,7] whose potential for use with x rays has been suggested previously by Huignard.[8] The two key components of a light valve are the photoconductor detector and the electro-optic light modulator, usually a liquid crystal (LC) cell, which are physically coupled in a sandwich structure, as shown in Fig. 1.

To sensitize the XLV to x rays, a potential is applied across the sandwich to create an electric field across the photoconductive layer. When incident x rays are absorbed in the photoconductor, electron-hole pairs are released, and subsequently the electrons and the holes are guided to the opposite surfaces of the photoconductor by the electric field. The presence of the electric field ensures that there is very little lateral spread in the charge movement, and thus the charge image collected at the photoconductor-LC interface faithfully reproduces the absorbed x-ray intensity pattern. The collected charges give rise to an electric potential across the LC cell, which changes the orientation of the liquid crystal molecules and affects the propagation of light from an external source through the LC cell. Thus spatial variations in the LC cell potential, in areas where x rays are absorbed, cause spatial variations in the intensity of the readout light transmitted through the LC cell. The XLV can be operated trans-

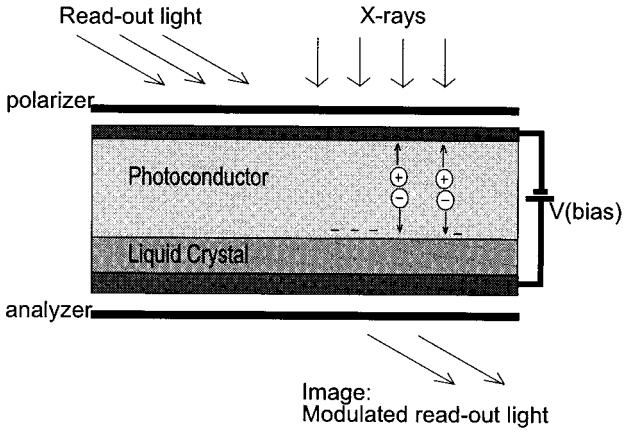

FIG. 1. A cross section of the structure of the x-ray light valve operated in a transmissive mode showing: a photoconductor and a liquid crystal cell physically coupled in a sandwich structure defined by transparent substrates with conductive surfaces connected to a bias potential; an external polarizer and analyzer and readout light; and the post-x-ray exposure movement of charge carriers, electrons, and holes, due to the presence of the electric field.

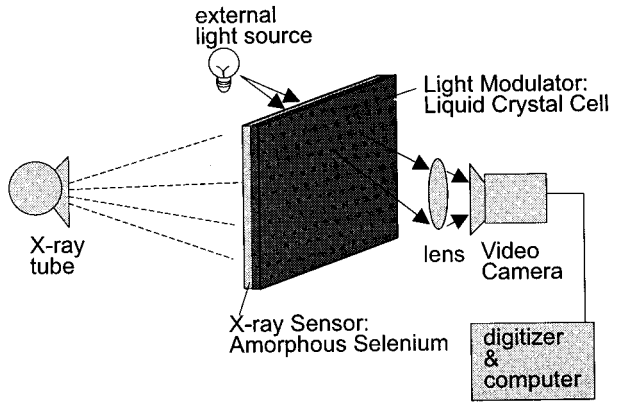

FIG. 2. The x-ray light valve imaging concept: x rays absorbed by the photoconductive detector activate the LC cell modulating the transmission of light from the external source. The light image is coupled via a lens to an optical detector, e.g., a CCD and the signal is subsequently digitized. Image brightness can be controlled independently from the exposure by adjusting the intensity of the light source and thus a secondary quantum sink may be avoided.

missively, with a readout light passing through both the photoconductor and the LC cell, provided that the light is nonactinic, i.e., of photon energy below the optical absorption edge of the photoconductor and thus unable to create electron-hole pairs). Alternatively the structure may include mirrored surfaces and a different polarizer arrangement for readout on the same side as illumination.[6]

Before a new exposure can be made it is necessary to wait for the image charge at the photoconductor-LC interface to discharge through the LC cell. To permit more rapid operation, the XLV may be reset. To do this the bias electric field is turned off, so that the only electric field is due to the image charge and the photoconductor is flooded with light. The released charges will move toward the interface to neutralize the remaining image charge. The bias field may then be reapplied and the device is ready to acquire a new image.

The XLV may be used for digital radiography in an arrangement illustrated in Fig. 2. Both the x rays and the readout light are incident from the photoconductor side of the XLV. The readout light is transmitted through the photoconductor and is spatially modulated in intensity by the LC cell to produce an image which is demagnified onto an optical imager such as a CCD camera using a lens. The CCD signal can be digitized subsequently. This simple scheme of digital image acquisition is possible because the XLV image is formed by x-ray exposure controlled modulation of light from an external source and the image brightness can be adjusted independently from the x-ray exposure. In other words, the XLV acts as an intensifier and loss of light via coupling optics can be compensated by increasing the readout light intensity. Therefore, the x-ray image can be recorded with an optical imager but without a secondary quantum sink under any demagnification. It should be noted that this is true only as long as the saturation signal level of the optical detector is high enough to not impose a limit on the quantum gain or the mapping between x-ray photons and the signal electrons in the XLV based imaging chain.[9]

The aim of this work is to model the XLV operation and to assess the feasibility of a practical XLV for radiography. We concentrate on the performance of the XLV: The complete imaging system consisting of an XLV coupled to a CCD camera has been previously discussed elsewhere.[9] To be applicable in clinical radiography, the XLV must satisfy certain criteria: The system must be sensitive enough to work within an acceptable range of diagnostic x-ray exposures; it must be x-ray quantum noise limited over this exposure range; and its resolution must be high. Mammography and chest radiography will be used as examples of possible imaging tasks as they encompass the extremes of resolution, exposure levels, and x-ray spectra required in radiographic procedures.

II. BACKGROUND

The two principal components of the XLV, the photoconductor x-ray detector and the electro-optic light modulator, are reviewed.

A. Photoconductor: Amorphous selenium

The XLV photoconductor must be sensitive to x rays, it must be capable of high resolution imaging, and it should have low dark current. Many photoconductors could be considered for use in the XLV but the characteristics of amorphous selenium (a-Se) make it particularly useful in this application. Large area a-Se detectors are also cost efficient and feasible because the photoconductor is amorphous and is made by evaporation techniques.

The clinical suitability of a-Se for medical x-ray imaging has been established previously in connection with xeroradiography[10] and digital radiography.[11] The x-ray sensitivity of a photoconductor depends on both the x-ray absorption, related to the atomic number and the thickness of the detector, as well as $W_{\pm}$, the energy required to release an electron-hole pair in the photoconductor. As an example of the x-ray absorption, one may consider 50-keV and 20-

keV x rays for which the linear attenuation coefficient, μ, of a-Se is 1.9×10^3 m^{-1} and 2.33×10^4 m^{-1}, respectively.[12] Thus 50% x-ray attenuation is achieved with a 365-μm-thick a-Se layer for a 50-keV beam and with a 30-μm-thick layer for a 20-keV beam. It has been shown experimentally that the $W_{\pm}$ of a-Se is a function of electric field, E, with the following dependency:[13]

$$W_{\pm}=50\left(\frac{E}{10}\right)^{\alpha}, \tag{1}$$

where α is ~-0.8 and at a typical bias electric field E of 10 V/μm, $W_{\pm}$ is $\sim$50 eV.[14] The ratio of x-ray photon energy, ξ, to $W_{\pm}$ can be thought of as the quantum gain in the photoconductor and at 10 V/μm for a-Se this gain is typically 400–1000 electrons/x ray, depending on the beam energy.

In electrostatic detectors the charge collection is guided by the presence of the electric field and there is very little resolution loss due to charge spread. The inherent spatial resolution limit of a-Se has been shown to be set by the x-ray interactions, namely the range of primary photoelectrons.[15] This makes a-Se a higher resolution detector than a phosphor screen whose resolution limit arises from optical spreading effects.[16]

Small and spatially uniform dark current in the photoconductor ensures that the dark current and its noise are negligible compared to the signal charge and its related noise. Provided the a-Se/substrate interface forms a charge blocking contact, the a-Se dark current can be kept small (resistivity $\sim10^{13}$–10^{14} Ωm)[17] at room temperature because it has a large band gap energy.

The proposed transmissive mode operation of the XLV requires use of nonactinic readout light. The absorption of a-Se drops quickly with wavelength (λ) greater than 700 nm, while the threshold of charge carrier photogeneration occurs at shorter λ.[17] Thus red/ir light (e.g., $\lambda>750$ nm) can be used as the readout light.

B. Electro-optic spatial light modulator: Twisted nematic liquid crystal cell

The electro-optic modulator of the XLV should be sensitive to small changes in potential and these changes should be fast and result in a light transmission versus potential characteristic that is monotonic and preferably linear. Fast response is required to permit rapid readout. Sensitivity is an issue since the XLV image charge, and thus the light modulator potential, is limited by the x-ray exposures that can be safely used in medical imaging. Linear response results in good contrast over a range of exposures but as long as the response is monotonic it can be linearized.

Different kinds of LC cells have distinctive characteristics.[18,19] Moreover, a variety of LC compounds have been developed to meet specific operational requirements (e.g., operating potential range).[20] The most common LC devices are based on the 90° twisted nematic mode. In these cells, light transmission varies monotonically over an applied potential range of a few volts. Furthermore, the characteristic is approximately linear in the 10%–90% transmission range. Figure 3 shows a theoretical characteristic curve of a twisted nematic LC cell.

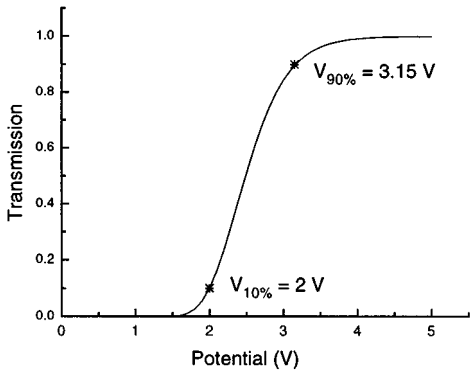

FIG. 3. Theoretical characteristic curve of a 90° twisted nematic LC cell operated in the normally black mode fitted to the 10% and 90% transmission values of Merck/BDH LC compound ZLI-0792.

LCs are organic molecules that exhibit an intermediate state of matter upon melting from a solid to a liquid. As the name implies, in the liquid crystalline phase the material shares some of the properties of liquids and some of those of solids: The molecules have short range orientational order similar to crystalline solids but lack long range order so that the material can flow like a liquid. LC molecules, often elongated in shape, have anisotropic physical properties such as the dielectric constant and the refractive index. The display applications of liquid crystal molecules are based on such anisotropies, which permit the molecular orientation to be manipulated by an applied electric field and so affect light propagation through the material. In particular, the twisted nematic mode relies on: (a) specific initial arrangement of the LC molecules; (b) the manipulation of the LC molecular alignment with an electric field; (c) the effect of the LC molecules on the polarization state of light.

The twisted nematic LC cell is constructed to have an initial helical molecular arrangement: The liquid crystal molecules lie parallel to the substrate electrodes with an in-plane orientation which twists from one substrate to the other, as shown in Fig. 4(a). The structure also includes a polarizer in the front of the cell and an analyzer in the rear. Such a cell functions as an optically active layer that rotates the plane of light polarization with the molecular twist. Thus the transmission of light is blocked by a 90° twisted nematic cell with the polarizer parallel to the analyzer, and the cell appears black. When a sufficient field is applied across the cell, the liquid crystal molecules align parallel to the electric field [Fig. 4(b)]. The helical structure and the rotation of light polarization are temporarily destroyed. Thus propagation of the polarized light is allowed by the analyzer and the cell appears bright. At intermediate potentials, the disruption in the helical arrangement is partial and shades of gray can be achieved. (Alternatively, the LC cell can be operated with a black signal on a clear background using perpendicular polarizer and analyzer arrangement.)

A theoretical model, developed by Lu and Saleh,[21] to pre-

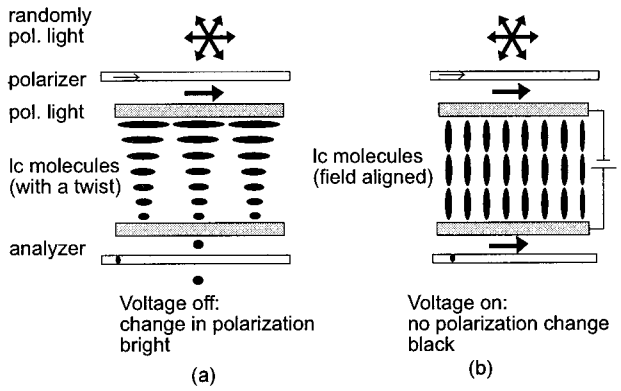

FIG. 4. Operation of a liquid crystal display in the normally black state: (a) no potential, helical molecular arrangement, off-state; (b) potential applied, field induced molecular arrangement, on-state.

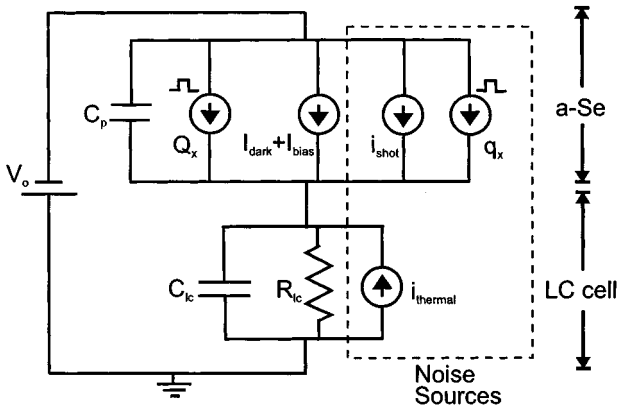

FIG. 5. Model equivalent electrical circuit of the x-ray light valve with elements corresponding to the components. The dotted section highlights the noise components.

dict the steady state optical response of the twisted nematic cell to an electric potential is outlined in the Appendix. This model can also be used to find the off-state transmission for the purposes of optimizing the LC cell design. The off-state transmission, T_{off} or the transmission in the absence of potential is given in terms of following variables: the LC birefringence, Δn, which is the difference between the indices of refraction along the long and the short axes of the LC molecule; the cell thickness, d_{LC}; and the wavelength of viewing light, λ. The following relationship has been found to give T_{off} for parallel arrangement of ideal polarizer and analyzer, i.e., for a normally black LC cell:[22]

$$T_{\text{off}}=\sin^2\left[\frac{\pi}{2}\sqrt{1+u^2}\right]/(1+u^2), \tag{2}$$

where $u=2d_{\text{LC}}\Delta n/\lambda$. The optimum cell contrast ratio $(1:T_{\text{off}})$ in this configuration is attained when the cell appears completely black in the off-state, i.e., T_{off} equals zero. This occurs at the minima of Eq. (2) when $u=\sqrt{3},\sqrt{15},\sqrt{35},...$ Operation at the first minimum is desired to keep the cell thickness as small as possible, as it has been shown that the LC cell response time increases as the square of the cell thickness.[18] Therefore the cell thickness should be

$$d_{\text{LC}}=\lambda\sqrt{3}/(2\Delta n). \tag{3}$$

In practice, the LC cell image quality and contrast ratio is also affected by the quality of the polarizers and the substrate LC molecule alignment layers, readout light intensity uniformity and spectral distribution, undesired light polarization effects (e.g., due to scattering at interfaces and in the bulk of LC cell), cell viewing angle, and variations in cell thickness.[22] Practical optimum contrast ratios may be in the range of 100:1 to 1000:1.[19]

III. MODEL OF THE XLV OPERATION

A model of the XLV operation was developed to predict its imaging properties and to optimize the photoconductor and LC cell parameters. The model covers the key aspects of a medical x-ray imaging system—sensitivity characteristic, noise, spatial resolution, NPS and spatial frequency dependent DQE, and temporal response.

Many of the calculations (MTF, DQF, NPS) are based on linear systems analysis while the XLV transmission may be a nonlinear function of the cell potential. Therefore to ensure linear analysis is applicable, such calculations will be carried out in the voltage domain.

It should also be noted that as the XLV is to be coupled with an optical detector such as a CCD, the operation of the complete XLV based imaging chain may be limited by the optical detector, namely its saturation signal, noise level, and the pixel count.[9]

A. XLV characteristic

The XLV response to x-ray exposures will be defined in terms of T_{XLV}, the characteristic curve of the XLV light transmission versus the incident x-ray exposure, X. To obtain this relationship, the LC response, i.e., the LC cell potential, V_{LC}, as a function of X is first calculated. This result is then substituted into the LC cell characteristic function, T_{LC}, i.e., the transmission versus potential as modeled in the Appendix, to obtain T_{XLV}.

The LC cell potential, V_{LC}, is determined using an equivalent electrical circuit model shown in Fig. 5. The electronic properties of the LC cell permit it to be represented as a resistance R_{LC} and a capacitance C_{LC} in parallel. (These, as all other physical properties of the XLV, are defined per unit area.) The photoconductive layer is represented by a capacitance C_p in parallel with a number of carrier sources; the dark current I_{dark}, the bias current I_{bias}, and the signal charge Q_x. The origin of I_{dark} is thermal excitation in the bulk or charge injection from the substrates, while the origins of I_{bias} and Q_x are optical and x-ray photon excitations, respectively. The noise currents and charges, i_{thermal}, i_{shot}, and q_x, are discussed in the next section.

First, the state of the LC cell prior to x-ray exposure, as shown in Fig. 6(a), will be established. The dc bias potential V_0 applied to the XLV results in a steady state V_{LC} that also depends on R_{LC} and I_{dark}. As can be seen in an LC cell

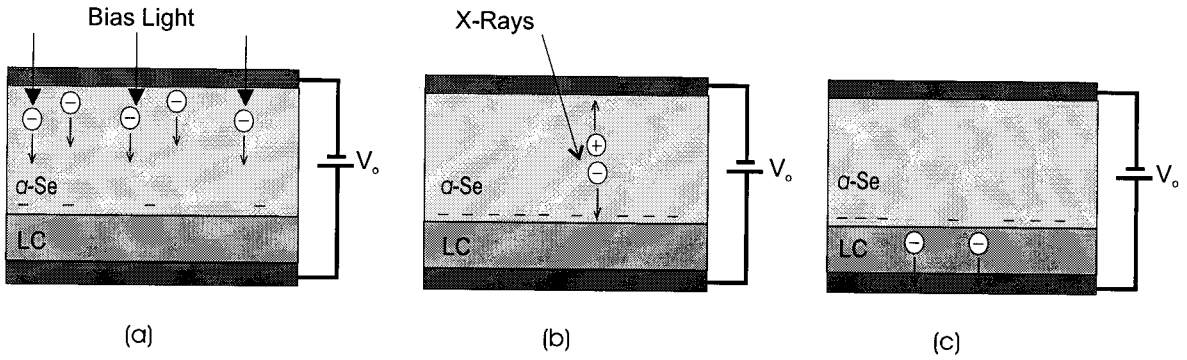

FIG. 6. The three stages of the x-ray light valve operation: (a) pre-exposure—the dark and bias currents, I_{dark} and I_{bias}, give rise to V'_{LC}; (b) the x-ray exposure gives rise to signal potential ΔV_{LC} and $V_{\text{LC}}=V'_{\text{LC}}+\Delta V_{\text{LC}}$; (c) post-exposure—exponential signal discharge, $V_{\text{LC}}=V'_{\text{LC}}+\Delta V_{\text{LC}}\exp(-t/\tau)$.

characteristic curve (Fig. 3), a threshold potential, V'_{LC} has to be reached before the optical state of the LC cell changes. However, I_{dark} is typically low and would result in a negligible V_{LC}. Therefore, to make efficient use of the x rays, the LC cell needs to be biased to V'_{LC} prior to the x-ray exposure. This is achieved with an additional current, I_{bias}, created by a controlled amount of actinic (e.g., blue) light incident on the photoconductor:

$$V'_{\text{LC}}=R_{\text{LC}}(I_{\text{bias}}+I_{\text{dark}}). \tag{4}$$

The bias light photon flux density, Φ, required to reach I_{bias} is obtained from:

$$\Phi=I_{\text{bias}}/(e\,\eta') \tag{5}$$

where e is the electron charge, and η' is the light photon quantum efficiency, i.e., number of charge quanta per absorbed photon. For blue light, η' for a-Se is approximately 50% at an electric field of 10 V/μm.[23]

Once biased electrically and optically, the XLV can be exposed with x rays as shown in Fig. 6(b). An exposure X of monoenergetic x rays gives rise to image charge Q_x at the interface between the a-Se and LC:

$$Q_x=XN_R\eta(\xi/W_{\pm})e, \tag{6}$$

where N_R is the number of photons per Roentgen, η is the x-ray quantum efficiency, ξ is the x-ray energy, and $\xi/W_{\pm}$ is the quantum gain or the number of electron-hole pairs released per x-ray photon. The charge Q_x is capacitively coupled between the two dielectric layers, the photoconductor and the LC cell, to give an additional exposure induced potential ΔV_{LC} across the LC cell due to the x-ray signal:

$$\Delta V_{\text{LC}}=Q_x/(C_{\text{LC}}+C_p). \tag{7}$$

By combining Eqs. (6) and (7), ΔV_{LC} is obtained as a function of exposure, and using the relationship $V_{\text{LC}}=V'_{\text{LC}}+\Delta V_{\text{LC}}$ the LC cell potential V_{LC} may be written as:

$$V_{\text{LC}}=V'_{\text{LC}}+\frac{XN_R\eta(\xi/W_{\pm})e}{C_p+C_{\text{LC}}}. \tag{8}$$

The XLV characteristic, T_{XLV}, i.e., the transmission as a function of x-ray exposure, can now be obtained: V_{LC} of Eq. (8) is combined with the LC cell light transmission characteristic, T'_{LC}, from the Appendix, to give

$$T_{\text{XLV}}=\frac{\pi\,\sin[\gamma(V_{\text{LC}})]}{\gamma(V_{\text{LC}})}, \tag{9}$$

where γ is a function of multiple LC variables as outlined in the Appendix.

B. Noise

The XLV noise sources can be separated into two types: the structural noise that arises from practical engineering limitations; and the fundamental noise due to the physical interactions. Structural noise in the XLV could arise from spatial variations in thicknesses and physical properties of the a-Se and LC layers or spatial variations in the readout light intensity. For example, the LC cell thickness, d_{LC}, has a direct effect on the electronic properties C_{LC} and R_{LC} and thus affects the signal potential ($\Delta V_{\text{LC}}\propto I/C_{\text{LC}}\propto d_{\text{LC}}$) and the LC bias potential ($V'_{\text{LC}}\propto R_{\text{LC}}\propto d_{\text{LC}}$). However, digital image acquisition should allow compensation of structural noise by background and gain calibration. Thus here only the fundamental sources of noise are considered in order to determine whether the XLV could be an x-ray quantum noise limited system.

In the circuit model (Fig. 5) the XLV noise is represented as a charge or current source: x-ray quantum noise charge, q_x; the shot noise current, i_{shot}; and thermal noise current, i_{thermal}. These noise sources differ in nature (charge versus current) and thus cannot be directly compared. However, as the LC cell acts as a charge integrator, both the charge and current sources give rise to LC cell potentials that can be directly compared and so used to analyze the significance of each of the noise sources. The effect of the system noise (comprising shot and thermal noises) and the x-ray quantum noise on the LC cell potential is shown qualitatively in Fig. 7, which shows V_{LC} as a function of time prior to and following an x-ray exposure.

The x-ray exposure gives rise to quantum noise which causes variation in the LC cell signal potential from exposure

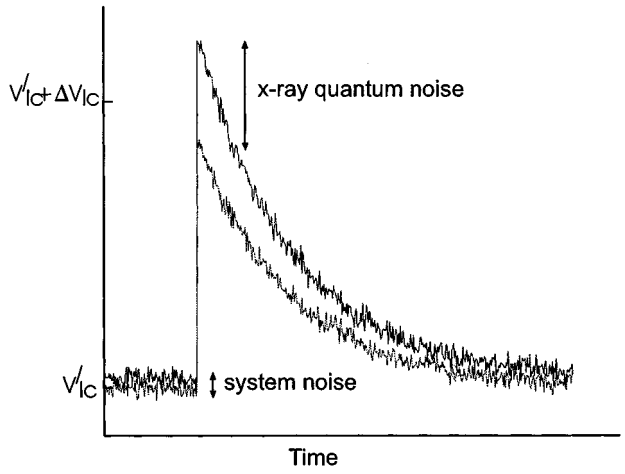

FIG. 7. Qualitative representation of the x-ray light valve signal, the x-ray quantum noise, and the system noise potentials at a particular pixel as a function of time for two different but nominally identical x-ray exposures.

to exposure or from point to point in the image. The x-ray statistics are governed by the Poisson distribution, which can be approximated by the Normal distribution, with $\sigma=\sqrt{N}$, when the number, N, of x rays in question is large (>20). Thus for a monoenergetic x-ray beam the standard deviation in the signal charge, or the quantum noise charge q_x, is given by the product of the square root of the number of x-ray quanta absorbed, the quantum gain, and the electron charge:

$$q_x=\sqrt{XN_R\eta}(\xi/W_{\pm})e. \tag{10}$$

The x-ray quantum noise charge gives rise to a potential across the LC cell in the same capacitive coupling manner [i.e., Eq. (7)] as the signal charge. Thus the standard deviation in the signal potential, which will be called the x-ray quantum noise potential ν_x, is

$$\nu_x=\frac{\sqrt{XN_R\eta}(\xi/W_{\pm})e}{C_{\mathrm{LC}}+C_p}. \tag{11}$$

The temporal variation in V_{LC} is due to the system noise, i_{shot} and i_{thermal}. These, initially white, noise sources are low pass filtered by the circuit formed by the elements R_{LC}, C_{LC}, and C_p with a 3-dB bandwidth $f_{3\text{-dB}}=1/[2\pi R_{\mathrm{LC}}(C_{\mathrm{LC}}+C_p)]$. The noise equivalent bandwidth, B, of such a low pass filter circuit is defined as $f_{3\text{-dB}}\pi/2$ and thus B is:[24]

$$B=\frac{1}{4R_{\mathrm{LC}}(C_{\mathrm{LC}}+C_p)}. \tag{12}$$

In principle, an observation or measuring interval must be defined as this effectively imposes another low pass filter on the system noise. However, in practice the measuring interval will be short relative to the RC time constant imposing an additional filter with a much higher noise bandwidth than B. Thus B remains the limiting bandwidth in the magnitude of the system noise.

Part of the system noise arises from the bias current, I_{bias}, which has shot noise due to the random nature of charge carrier generation in the photoconductor. The rms shot noise current, i_{shot} is given by:[24]

$$i_{\mathrm{shot}}=\sqrt{2eI_{\mathrm{bias}}B}. \tag{13}$$

Thermal (Johnson) noise in the LC cell also contributes to system noise and the corresponding noise current, i_{thermal}, is given by

$$i_{\mathrm{thermal}}=\sqrt{kTB/R_{\mathrm{LC}}}, \tag{14}$$

where k is Boltzmann's constant, and T is absolute temperature. These rms system noise currents flow through R_{LC} and are converted into rms noise potentials whose value is obtained using Ohm's law. The thermal and shot noise potentials, ν_{thermal} and ν_{shot}, which together comprise the system noise, ν_{system} are uncorrelated and can be therefore added in quadrature. Using Eqs. (13) and (14) and Ohm's law, ν_{system} can be written as

$$\nu_{\mathrm{system}}=\sqrt{2eI_{\mathrm{bias}}BR_{\mathrm{LC}}^2+kTBR_{\mathrm{LC}}}. \tag{15}$$

C. The exposure range

The quantum limited exposure range will be defined as the range of exposures from the minimum exposure, at which the XLV is still x-ray quantum noise limited, to the maximum exposure permitted before LC cell saturation. The minimum exposure, X_{min}, can be determined using Eqs. (11) and (15) to solve for the exposure at which ν_x equals ν_{system}:

$$X_{\mathrm{min}}=\frac{(C_{\mathrm{LC}}+C_p)^2\nu_{\mathrm{system}}^2}{N_R\eta[(\xi/W_{\pm})e]^2}. \tag{16}$$

The maximum exposure is obtained from Eq. (8) by solving for the exposure, X_{max} at which the cell potential equals the saturation level of the LC cell, i.e., $V_{\mathrm{LC}}=V_{\mathrm{LC}}^s$:

$$X_{\mathrm{max}}=\frac{(V_{\mathrm{LC}}^s-V_{\mathrm{LC}}')(C_p+C_{\mathrm{LC}})}{N_R\eta(\xi/W_{\pm})e}. \tag{17}$$

D. Spatial resolution

The resolution of the XLV depends on both the inherent resolution of the photoconductor detector in bringing charge to the photoconductor-LC cell interface as well as the resolution of the charge readout. The inherent resolution of a-Se has been analyzed previously[15] and the resulting photoconductor modulation transfer function, MTF_p, will be incorporated in the resolution model of the XLV.

The XLV optical response arises from the cell potential induced by the spatial charge distribution at the photoconductor-LC interface. The corresponding readout resolution, described by MTF_v, is obtained by calculating the LC cell potential modulation, at a given spatial frequency, and by normalizing the result by the cell potential modulation at zero spatial frequency. The modulation of the LC cell potential depends on the distribution of electric fields in the two dielectrics, the a-Se photoconductor and the LC

cell. The XLV electric fields, and thus the interface potential, can be found by solving Laplace's equation with the appropriate boundary conditions: the biased and the grounded substrates, and the interface charge distribution. Here the solution for Laplace's equation as derived by Schaffert[25] for a charge distribution at the interface of two dielectrics sandwiched between electrodes is used.

The final XLV signal transfer can then be described by $\mathrm{MTF}_{\mathrm{XLV}}$ as follows:

$$\mathrm{MTF}_{\mathrm{XLV}}=\mathrm{MTF}_p\mathrm{MTF}_v\,. \tag{18}$$

$\mathrm{MTF}_{\mathrm{XLV}}$ is independent of the exposure level as long as the signal charge is small enough not to affect the magnitude of the bias electric field in the photoconductor significantly as this would alter the quantum gain.

E. The noise power spectra and the spatial frequency dependent detective quantum efficiency

The noise transfer through the XLV will be studied in terms of the noise power spectrum, NPS, and the signal to noise ratio, SNR, transfer will be expressed in terms of the detective quantum efficiency, DQE. The NPS and the DQE are functions of both spatial frequency and exposure.

The XLV noise power spectrum, $\mathrm{NPS}_{\mathrm{XLV}}$, can be obtained by summing the NPS of each individual noise source. All are white at source but are subject to spatial modulation as follows: The x-ray quantum noise arises at the input of the XLV, is spatially transferred through the complete system, and is hence modified by $\mathrm{MTF}_{\mathrm{XLV}}$; thermal noise is spatially bandwidth limited only by the readout MTF_v; and the shot noise transfer is given in terms of the product $\mathrm{MTF}'_p\mathrm{MTF}_v$, where MTF'_p is due to spread in optically induced photoconductor charge. As MTF'_p is essentially unity up to very high spatial frequencies,[25] the product $\mathrm{MTF}'_p\mathrm{MTF}_v$ can be approximated as MTF_v. Thus by adding the shot and thermal noise sources in quadrature to give ν^2_{system} the NPS for the complete XLV imaging system is

$$\begin{aligned}\mathrm{NPS}_{\mathrm{XLV}}&=\nu_x^2\mathrm{MTF}_{\mathrm{XLV}}^2+\nu_{\mathrm{shot}}^2\mathrm{MTF}_v^2+\nu_{\mathrm{thermal}}^2\mathrm{MTF}_v^2\\&=\nu_x^2\mathrm{MTF}_{\mathrm{XLV}}^2+\nu_{\mathrm{system}}^2\mathrm{MTF}_v^2.\end{aligned} \tag{19}$$

In general, the DQE may be expressed in terms of: S, the system response to the incident quanta; the MTF; the noise power spectrum, NPS; and the number of incident quanta, N.[11]

$$\mathrm{DQE}=[S^2\mathrm{MTF}^2/\mathrm{NPS}]/N. \tag{20}$$

The response S will be expressed in terms of the LC cell signal potential ΔV_{LC} from Eq. (7), and the product of exposure, X, and number of photons per Roentgen, N_R, gives N. Thus $\mathrm{DQE}_{\mathrm{XLV}}$ can be expressed as

$$\mathrm{DQE}_{\mathrm{XLV}}=\frac{\Delta V_{\mathrm{LC}}^2\mathrm{MTF}_{\mathrm{XLV}}^2}{(\nu_x^2\mathrm{MTF}_{\mathrm{XLV}}^2+\nu_{\mathrm{system}}^2\mathrm{MTF}_v^2)XN_R}. \tag{21}$$

F. XLV temporal properties

The signal potential across the LC cell due to an x-ray exposure varies with time and, as will be shown, this temporal property of the XLV provides a unique means to extend the exposure latitude. To understand the temporal response of the XLV, several simplifying assumptions are made. The x-ray exposure is assumed to be instantaneous with respect to the XLV response, and the response time of the photoconductor (<1 ms)[18] and the signal dependent LC response time[18] ($\sim$10–100 ms) will be ignored on the basis that the response due to the integrating properties of the XLV will dominate the total response time.

As shown in Fig. 6(c), the signal charge collected at a-Se/LC interface discharges through the LC. This can be modeled as a ΔV_{LC} decrease (Fig. 7) as the signal charge, Q_x, stored on XLV capacitance $(C_{\mathrm{LC}}+C_p)$ dissipates through R_{LC} at a rate governed by the RC time constant $\tau=R_{\mathrm{LC}}(C_{\mathrm{LC}}+C_p)$. The LC cell signal potential, ΔV_{LC}, is thus a function of post-exposure time t and thus the time dependent LC cell potential, $V_{\mathrm{LC}}(t)$, is

$$V_{\mathrm{LC}}(t)=V'_{\mathrm{LC}}+\Delta V_{\mathrm{LC}}\exp(-t/\tau). \tag{22}$$

The decrease in ΔV_{LC} with time implies that each x-ray exposed area exhibits variation in transmission as the XLV returns to its pre-exposure state. This phenomenon may be examined further in terms of the XLV characteristic. The XLV characteristic, T_{XLV}, can also be written as a function of t by substituting Eq. (22) into Eq. (9).

The upper limit of the time dependent exposure range, $X_{\max}(t)$, is obtained by equating $V_{\mathrm{LC}}(t)$ of Eq. (22) with the saturation potential V^s_{LC} and simplifying the result by equating $X_{\max}(t=0)$ to $X_{\max}$ from Eq. (17):

$$X_{\max}(t)=X_{\max}(0)\exp(t/\tau). \tag{23}$$

The lower limit of the exposure range, $X_{\min}(t)$, can be found by examining noise as a function of time. Because the x-ray induced signal potential decreases exponentially in time, the magnitude of the x-ray quantum noise, $\nu_x(t=0)$ equal to ν_x from Eq. (11), also decays exponentially:

$$\nu_x(t)=\nu_x(0)\exp(-t/\tau). \tag{24}$$

However, the magnitude of the system noise, ν_{system}, is time independent. By equating $\nu(t)$ to ν_{system} and simplifying the result using $X_{\min}\,(t=0)$ equal to $X_{\min}$ from Eq. (16), one can solve for $X_{\min}(t)$, the minimum exposure that leads to x-ray quantum noise limited operation at time t after the exposure:

$$X_{\min}(t)=X_{\min}(0)\exp(2t/\tau). \tag{25}$$

Similarly, the $\mathrm{NPS}_{\mathrm{XLV}}$ and $\mathrm{DQE}_{\mathrm{XLV}}$ must now be expressed as time dependent functions. As the ratio of the x-ray quantum noise to the system noise varies with time, $\mathrm{NPS}_{\mathrm{XLV}}$ can also be written as a time dependent function by substitution of $\nu_x(t)$ into Eq. (19):

$$\mathrm{NPS}_{\mathrm{XLV}}(t)=\nu_x(t)^2\mathrm{MTF}_{\mathrm{XLV}}^2+\nu_{\mathrm{system}}^2\mathrm{MTF}_v^2. \tag{26}$$

The time dependent $\mathrm{DQE}_{\mathrm{XLV}}(t)$ can be expressed in terms of exponentially decaying ΔV_{LC} and ν_x and is obtained by substitution of $\Delta V_{\mathrm{LC}} \exp(-t/\tau)$, and $\nu_x(t)$ into Eq. (21):

$$\mathrm{DQE}_{\mathrm{XLV}}(t) = \frac{\Delta V_{\mathrm{LC}}^2 \exp(-2\tau/t)\mathrm{MTF}_{\mathrm{XLV}}^2}{[\nu_x(t)^2 \mathrm{MTF}_{\mathrm{XLV}}^2 + \nu_{\mathrm{system}}^2 \mathrm{MTF}_V^2] X N_R}. \quad (27)$$

Suitable times at which to examine the time dependent XLV parameters depend on the exposure range of interest. Three image acquisition times will be considered as examples: time zero that corresponds to the highest operating sensitivity; time $t_{\max}$ when the signal at the maximum clinical exposure, $X_{\max}^c$, has decayed to coincide with the LC cell saturation threshold, V_{LC}^s and an intermediate time $t_{\max}/2$. Time $t_{\max}$ is the latest image acquisition time and thus represents the worst case scenario in terms of the ratio of x-ray quantum noise versus system noise. Using Eq. (23), $t_{\max}$ can be solved for by equating $X_{\max}^c = X_{\max}(t)$ and substituting $X_{\max}$ from Eq. (17) into the result:

$$t_{\max} = \ln\left[\frac{X_{\max}^c N_R \eta(\xi/W_{\pm})e}{(V_{\mathrm{LC}}^s - V'_{\mathrm{LC}})(C_{\mathrm{LC}} + C_p)}\right]. \quad (28)$$

IV. APPLICATIONS

The model of the XLV operation was applied with x-ray beam parameters based on two particular imaging tasks: chest imaging and mammography. The calculations were based on monoenergetic beams approximating the mean energies of commonly used x-ray spectra; 50 keV for chest and 20 keV for mammography.[26] The means of the clinical exposures, X^e, expected at the detector were taken to be 10 mR for mammography[27] and 300 μR for chest,[28] with an exposure range of 1/10 to 10 times the average exposure. The number of photons per Roentgen, N_R, for 20-keV and 50-keV beams is 5.493×10^{13} m^{-2} and 2.842×10^{14} m^{-2}, respectively.[29]

A number of variables must be considered in the design of the XLV. The most fundamental of these are the kind of photoconductor, its thickness, and the kind of LC material used. The physical properties of the chosen materials define the electrical properties used in the model.

Here the thickness of the XLV a-Se layer was chosen to be 500 μm. At this thickness of photoconductor, both of the imaging tasks above would have adequate quantum efficiencies (99.9% with 20-keV x rays and 51.7% with 50-keV x rays). If the a-Se electric field is 10 V/μm, $W_{\pm}$ is $\sim$50 eV which results in a quantum gain of 400 electrons/x ray and 1000 electrons/x ray with 20-keV and 50-keV x rays, respectively. This field and photoconductor thickness imply a bias potential, $V_0 = 5000$ V. The photoconductor capacitance is also required for signal calculation: The relative dielectric constant of a-Se, ϵ_p, is 6.3 which makes $C_p = 1.1\times10^{-7}$ F/m^2.

An important requirement for the XLV is a sufficient RC time constant, τ, so that the image can be captured before the signal decays as predicted by Eq. (22). Although the photoconductor and the LC dielectric constants are typically comparable, the LC cell is much thinner than the photoconductor and hence $C_{\mathrm{LC}} \gg C_p$ and $\tau \sim R_{\mathrm{LC}} C_{\mathrm{LC}}$. Because the relative dielectric constants do not vary much between different LC materials, the adjustable parameter controlling τ is the resistance of the LC material, R_{LC}. Thus to prevent fast image discharge, a high resistivity or a ''high holding'' LC material must be chosen.

TABLE I. Model calculations parameters and results for system response, quantum limited exposure range, and image acquisition time $t_{\max}$ for an XLV biased at 1.35 V for the mammography and chest imaging examples.

Property	Mammography	Chest imaging
Mean energy	20 keV	50 keV
Quantum efficiency	99.9%	57.1%
Clinical exposure range, X^e	1–100 mR	30–3000 μR
System response	0.46 V/mR	3.40 V/mR
$X_{\min}$ $(t=0)$	3.7 μR	0.2 μR
$X_{\max}$ $(t=0)$	4.0 mR	530 μR
$t_{\max}$	16.6 s	8.9 s

Here calculations were based on ZLI-4792, an LC compound manufactured by Merck/BDH with the following nominal properties: anisotropy in the index of refraction $\Delta n = 0.0969$; an average relative dielectric constant $\epsilon_{\mathrm{LC}} = 5.7$; resistivity $\sigma_{\mathrm{LC}} > 10^{10}\,\Omega$m; and 10%–90% transmission operating range from 2V to 3.15 V.[20] The appropriate d_{LC}, from Eq. (3), for viewing at $\lambda = 750$ nm is 6.7 μm. Thus LC cell unit area capacitance $C_{\mathrm{LC}} = 7.6\times10^{-6}$ F/m^2, and when resistivity σ_{LC} was taken to be $10^{11}\,\Omega$m, the resistance $R_{\mathrm{LC}} = 6.7\times10^5\,\Omega$m^2, and therefore a RC time constant $\tau \sim 5$ s.

The a-Se and LC cell parameters above were used in the model to predict the XLV operation. First the static, $t=0$, behavior was analyzed in terms of the transmission characteristic, noise, exposure range, resolution, NPS, and DQE. Then the XLV temporal properties were included in the calculations, and the results were reexamined as most of the operating properties are time dependent.

V. RESULTS AND DISCUSSION

A. XLV characteristic, noise, and exposure range

First the LC cell characteristic T_{LC}^V was calculated by adjusting parameters in the LC cell transmission model (see the Appendix) to obtain an agreement between the model characteristic and the nominal 10% and 90% transmission potentials of the choser LC material. A fit, shown in Fig. 3, was obtained with the two adjustable transmission model parameters, V_{th} and V_{mid} set to values 1.35 V and 1.26 V, respectively. The required bias current and corresponding bias light flux were then calculated using Eqs. (4) and (5). V'_{LC} is chosen to equal V_{th}, I_{dark} is assumed to be negligible, and thus $I_{\mathrm{bias}} = 2.0\ \mu$A/m^2. This corresponds to a flux density $\Phi \sim 2.5\times10^{12}$ photons/m^2 s of blue light photons with an irradiance of $\sim 13\ \mu$W/m^2.

The magnitude of the LC signal potential, ΔV_{LC} was calculated as a function of exposure for the mammographic (20 keV) and chest imaging (50 keV) beams using Eqs. (6) and (7) to obtain the system response given in Table I. The LC

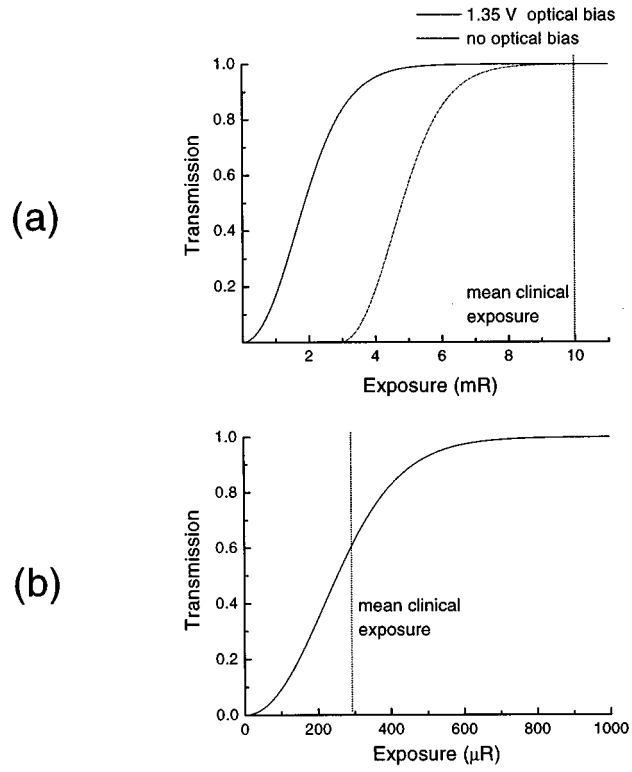

FIG. 8. The characteristic curve, T_{XLV}, of the x-ray light valve at $t=0$ for: (a) an optically biased and unbiased system for mammography; (b) an optically biased system for chest imaging.

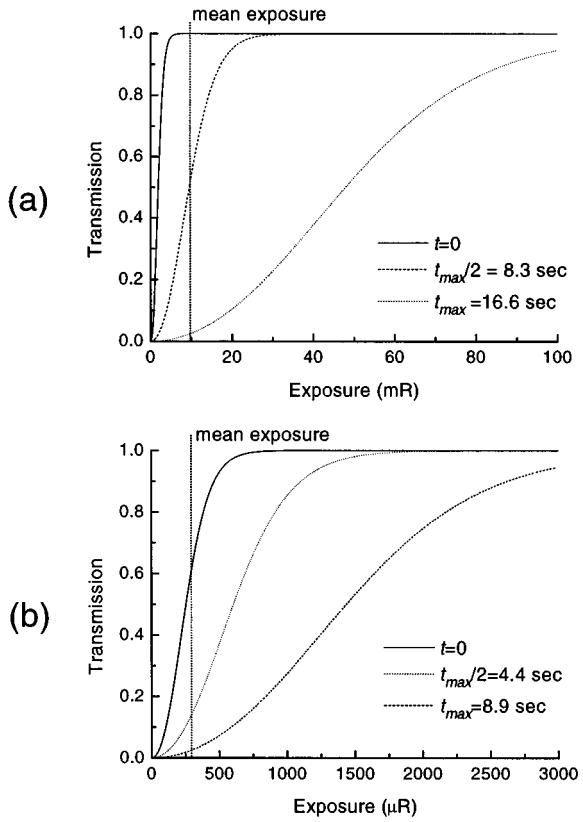

FIG. 9. The characteristic curve, T_{XLV}, of an optically biased x-ray light valve at various times after the x-ray exposure for: (a) mammography; (b) chest imaging.

cell potential, V_{LC}, calculated from Eq. (8), was then combined with T_{LC}^{V} (see the Appendix) to obtain the transmission versus exposure characteristic T_{XLV} for the optically biased XLV, as shown in Fig. 8. In addition, the limits X_{min} and X_{max} of the quantum limited exposure range were calculated using Eqs. (16) and (17), and are also summarized in Table I.

The calculations of S (Table I) indicate that the XLV is sensitive to x-ray exposures within the clinically relevant range. Furthermore, the calculated X_{min} shows that at its most sensitive, at $t=0$, the XLV is quantum noise limited to exposures well below the clinical exposures in both mammography and chest imaging. The relatively low XLV system noise is explained by the simple structure and the lack of external electronics, e.g., switching elements, amplifiers, or long electrodes.

As seen in Table I, at $t=0$ the XLV has been found to have approximately three orders of magnitude quantum noise limited exposure range. Results of Fig. 8(b) and Table I also show that the XLV characteristic for chest imaging is close to fulfilling the clinical exposure range requirements. However, the predicted exposure range for the XLV [Fig. 8(a)] for mammography does not coincide with the clinical exposure range. The higher mammographic exposures would result in signal potential, ΔV_{LC}, of the order of tens of volts which would saturate the LC cell.

Thus to better match the requirements of mammography, the signal handling capability of the XLV has to be increased. One way this may be achieved is to decrease the sensitivity by reducing the photoconductor quantum gain: Lower bias electric field in the photoconductor would increase $W_{\pm}$, the energy required to produce an electron-hole pair [Eq. (1)], and thus decrease the gain, $\xi/W_{\pm}$, and the signal potential ΔV_{LC}. The limit to such bias field reduction in a-Se arises from the increase in charge trapping which can lead to ghost images and loss of resolution.[18]

Perhaps a more important way by which the exposure range of the XLV can be extended arises from its temporal properties. A set of XLV characteristics, $T_{XLV}(t)$, can be obtained at different post-exposure times, e.g., $t=0$, $t_{max}/2$, and t_{max}. First t_{max} was calculated using Eq. (28), and $T_{XLV}(t)$ was obtained using Eq. (22) and T_{LC}^{V} (see the Appendix) for the optically biased XLV under mammographic and chest imaging exposures. The set of $T_{XLV}(t)$, given in Fig. 9, shows that the XLV characteristic depends greatly on the post-exposure time at which the image is observed. The image acquisition time may thus be chosen to obtain an image with the desired exposure to transmission mapping. Alternatively the image may be read out multiple times, and thus a single x-ray exposure can be used to obtain a temporal series of images, each of which exhibits high contrast over a different exposure range.

The time dependent, quantum limited exposure range is plotted in Fig. 10 and shows $X_{max}(t)$ and $X_{min}(t)$, from Eqs. (23) and (25), as a function of time for mammography and chest imaging. Because $V_{LC}(t)$ decreases with t, the effective quantum gain of the XLV decreases with t, and the

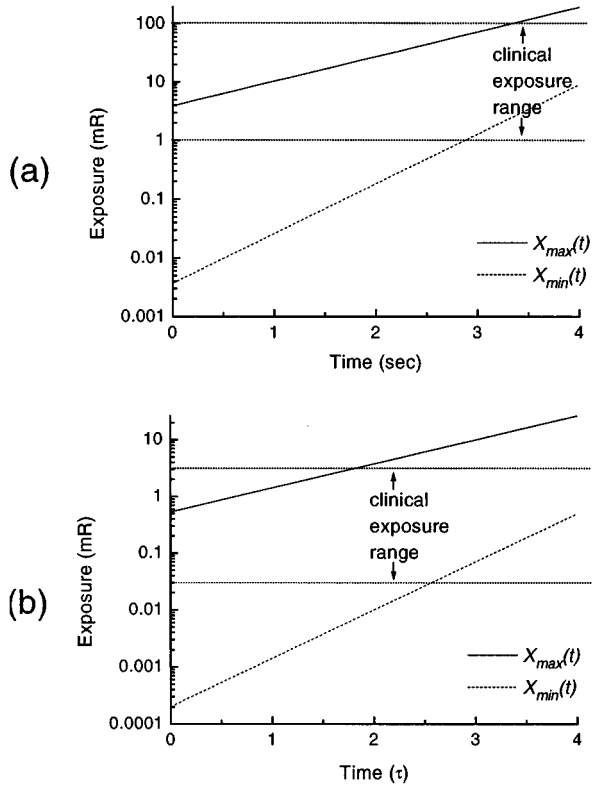

FIG. 10. The quantum limited exposure range of an optically biased x-ray light valve, from $X_{\min}$ to $X_{\max}$, as a function of post-exposure time for: (a) mammography; (b) chest imaging.

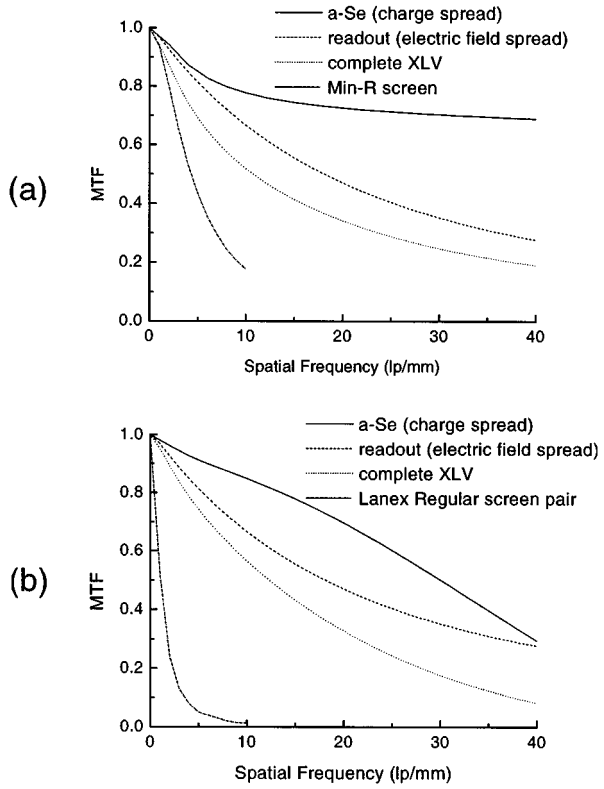

FIG. 11. The x-ray light valve resolution: components of MTF_{XLV} (the *a*-Se, the charge readout, and the total system MTF), and for comparison the MTF of an appropriate phosphor screen in the case of: (a) mammography; (b) chest imaging.

magnitude of the x-ray quantum noise potential decreases with respect to the system noise. Thus the minimum exposure $X_{\min}(t)$, at which the quantum noise matches the system noise, increases exponentially with t. Similarly $X_{\max}(t)$ also increases with t but at a different rate (increasing exponentially with $2t$) as illustrated in Fig. 10. Therefore, although the exposure range shifts to higher exposures with time, the relative exposure latitude, or the ratio of $X_{\max}(t)$ to $X_{\min}(t)$, decreases exponentially.

In the case of mammography, T_{XLV} was also obtained for the optically unbiased XLV and is shown in Fig. 8(a). As seen by comparison of the two characteristics, one for the optically biased and the other for the unbiased XLV, the choice of bias conditions used to bring the LC cell to the threshold, V'_{LC}, of its operation affects T_{XLV}: A change in the bias potential results in a shift of T_{XLV} along the exposure axis. This may be used, in conjunction with the time dependent exposure range, to optimize the XLV operation to a specific imaging task.

B. Spatial resolution

To obtain the resolution of the signal charge readout, MTF_v, Schaffert's solution[25] for Laplace's equation was applied to the XLV geometry. To obtain the *a*-Se charge spread resolution, MTF_p, the theoretical results by Que *et al.* for normally incident x rays of energies 20 keV and 50 keV[15] were used. Figure 11 shows MTF_v, MTF_p, and the product of these, the complete system MTF_{XLV} at the two beam energies.

The model indicates that the XLV should easily provide the resolution needed for these clinical radiologic tasks. The MTF_{XLV} [Fig. 11(a)] at mammographic x-ray energies greatly surpasses that of a typical mammographic screen[30] shown for comparison. The same is true for chest imaging as seen by comparison of MTF_{XLV} and the MTF of a typical chest screen[31] in Fig. 11(b). Moreover, high XLV resolution is attained with photoconductive detectors thick enough to have high quantum efficiency.

The limiting factor in the XLV resolution was found to be the charge readout resolution, MTF_v, which is determined by the thickness and the dielectric constant of the LC cell. However, as stated above, the XLV will require an optical imager such as a CCD array to complete the imaging system, and the final image resolution will also depend on the optical imager and the demagnification optics used.[9]

C. NPS and spatial frequency dependent DQE

To study the significance of the various noise sources at all spatial frequencies, the magnitudes of system and x-ray quantum noise potentials, ν_x and ν_{system} from Eqs. (11) and (15), were combined with the appropriate MTFs [Eq. (19)] to obtain the noise power spectra shown in Fig. 12. Comparison of the NPS of the x-ray quantum noise (at $X_{\min}$ and $X_{\max}$), and the system noise indicates that the x-ray quantum noise

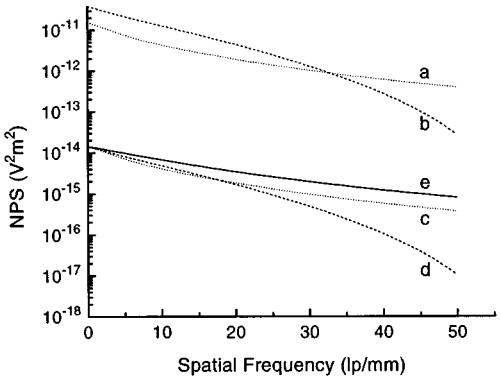

FIG. 12. Comparison of the x-ray light valve NPS corresponding to the system noise and the x-ray quantum noise at the limits of the quantum limited exposure range at $t=0$: (a) quantum noise at X_{max} (4 mR) for mammography; (b) quantum noise at X_{max} (0.53 mR) for chest imaging; (c) quantum noise at X_{min} (3.7 μR) for mammography; (d) quantum noise at X_{min} (0.2 μR) for chest imaging; (e) system noise.

continues to dominate up to high spatial frequencies except when exposures approach X_{min} and the quantum noise approaches system noise.

As the XLV is quantum noise limited over a large range of operating conditions, the SNR is also transferred efficiently. This can be seen in the DQE_{XLV} calculated using Eq. (21) for both 20-keV and 50-keV beams at X_{min} and X_{max} and plotted in Fig. 13. The DQE_{XLV} remains constant and close in value to the quantum efficiency over spatial frequencies of interest at high exposures. Even when exposures approach the quantum limit, X_{min}, the DQE is comparable or better than those of presently used radiographic systems, for example, stimulable phosphor systems used in chest imaging[32] and film-screen[30] combinations used in mammography. The phosphor based systems have a lower zero spatial frequency DQE that also decreases much faster than DQE_{XLV} with increasing spatial frequency. The XLV performs well in terms of the DQE since its quantum efficiency can be made high, the system noise is low, and because the NPS of the quantum noise dominates over the NPS of the system noise at all spatial frequencies of interest. Thus an XLV based radiographic system has the potential to reduce the image noise and hence permit exposure reduction compared to systems in current use.

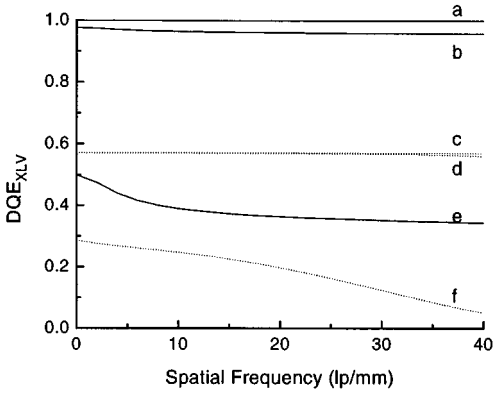

FIG. 13. Detective quantum efficiency, DQE_{XLV}, of the x-ray light valve for: (a) mammography at $X_{max}(t=0)$; (b) mammography at $X_{max}(t_{max})$; (c) chest imaging at $X_{max}(t=0)$; (d) chest imaging at $X_{max}(t_{max})$; (e) mammography at X_{min}; and (f) chest imaging at X_{min}.

Figure 13 also shows how changes in image acquisition time alter DQE_{XLV}. Here $DQE_{XLV}(t_{max})$ was calculated from Eq. (27) for both 20-keV and 50-keV beams at the corresponding maximum exposure, $X_{max}(t_{max})$, from Eq. (23). Comparison of the DQE curves at $t=0$ and $t=t_{max}$ shows some degradation of DQE_{XLV} with time. This is expected since the system quantum gain is effectively time dependent due to the discharge of the LC cell signal and the relative magnitude of the quantum noise decreases with respect to the system noise. The temporal DQE degradation implies that although different exposures map to the optimum contrast range of the XLV at different times, the image quality at different times may vary slightly. [The DQE at $X_{min}(t)$ remains constant by definition as this is the exposure at which system noise and quantum noise are equal.]

These DQE calculations do not take into account the effect on zero spatial frequency noise of the inherent variations in the photoconductor gain due to factors such as fluorescence escape, described by the Swank factor. However, Fahrig *et al.*[33] predict the Swank factor to be greater than 0.9 for *a*-Se plates thicker than 300 μm exposed to x rays in the diagnostic energy range. Thus the Swank factor should not decrease the calculated DQE_{XLV} by more than 10%.

VI. CONCLUSIONS

A theoretical feasibility study of a novel flat panel radiographic imaging system, the x-ray light valve, or XLV, has been presented. The model developed indicates that the XLV can, in principle, satisfy or exceed the requirements of clinical imaging in terms of its sensitivity, resolution, and noise. However, almost all the key operating parameters depend on a number of adjustable variables, namely the image acquisition time, the LC cell bias, and the photoconductor gain. Thus properties, such as the operating characteristic, can be optimized for a desired imaging task by choosing the appropriate operating conditions, and a single XLV unit may be used in diverse imaging tasks.

The XLV is essentially an image intensifier that can be used to construct an optically coupled digital radiographic system without a secondary quantum sink. Moreover, since the XLV is based on an electrostatic x-ray detector (*a*-Se), high image resolution can be achieved with detectors thick enough to provide high quantum efficiency. Thus an XLV based imaging chain may overcome some of the limitations typical of phosphor screen based digital imaging systems. In addition, as the XLV structure is simple, both the photoconductor detector and the LC light modulator are based on well established technologies, and little external circuitry or mechanical support is required, the manufacturing cost of the XLV could be kept low. Thus one may predict that a properly optimized XLV could be a versatile, inexpensive, high quality imaging system, and thus an attractive alternative for radiology departments globally.

ACKNOWLEDGMENTS

We gratefully acknowledge discussion with Dr. Birendra Bahadur of Litton Systems Canada, André Mouton of Noranda Advanced Materials, David Hunter and other members of our research team. We thank the Medical Research Council of Canada for financial assistance.

APPENDIX: THE LC CELL CHARACTERISTIC CURVE

The LC cell transmission characteristic is obtained using a model developed by Lu and Saleh[21] and later further expanded by Soutar and Lu.[34] The model combines (a) molecular orientation as a function of electric potential and (b) light transmission as a function of molecular orientation.

The LC molecular orientation is a function of the cell potential and may be calculated via minimization of LC cell elastic and electric energies. Lu and Saleh have obtained a first approximation analytical function to give the molecule tilt angle, θ, by ignoring the effect of substrate anchoring and assuming that all molecules tilt in similar fashion in the presence of an electric field:

$$\theta = \frac{\pi}{2} - 2\tan^{-1}\exp\left[-(V_{\mathrm{LC}} - V_{\mathrm{th}})/V_{\mathrm{mid}}\right], \tag{A1}$$

where V_{LC} is the LC cell potential, V_{th} is the threshold potential for molecule tilt, and V_{mid} is the potential above V_{th} at which the tilt angle is 49.6°. The tilt angle, θ, varies from 0° (molecules parallel to the substrate) to 90° (molecules perpendicular to the substrate). Equation (A1) holds for $V_{\mathrm{LC}} > V_{\mathrm{th}}$: for potentials below V_{th}, the tilt angle is zero.

Next Jones calculus, a well established optics tool, is used to obtain light transmission as a function of molecular orientation. The basis of this method is to create a matrix to describe transfer of light polarization through each component of the optical chain: Matrix, A, for the analyzer; and a matrix LC for the LC cell. A vector, E_{out}, which describes the polarization state of the emerging light is obtained by multiplication of the Jones matrices with the incident light vector, E_{in}. In the case where the polarizer, and thus incident light polarization, on the input face of the LC cell is parallel to the LC molecule long axis, and the analyzer is parallel to LC molecule long axis in the exit face of the cell, the following gives E_{out}:

$$E_{\mathrm{out}} = A * LC * E_{\mathrm{in}}, \tag{A2}$$

where A and E_{in} are:

$$A = \begin{bmatrix} 1 & 0 \\ 0 & 1 \end{bmatrix} \quad E_{\mathrm{in}} = \begin{bmatrix} 1 \\ 0 \end{bmatrix}. \tag{A3}$$

The LC cell transmittance, T, i.e., the emerging light intensity, is then the square of the magnitude of the vector E_{out}:

$$T = |E_{\mathrm{out}}|^2. \tag{A4}$$

To obtain the LC cell Jones matrix, LC, the cell can be divided into a set of parallel plates, each of which has molecule orientation twisted by an infinitesimal angle from the previous layer.[35] The twist angle increases incrementally from layer to layer for a total angle, α, from one substrate to another. With the twisted nematic cells α is typically 90°. Each layer acts as a birefringent crystal and gives rises to a relative phase difference between the components of light going through it. In the absence of potential, the birefringence arises from the difference between the refractive indices along the ordinary (short) and extraordinary (long) axis of the molecules, n_0 and n_e. However, as the molecule tilt angle, θ, increases with potential [Eq. (A1)], the effective extraordinary refractive index in the layer plane, $n_e(V)$, changes and one may write $n_e(V)$ as

$$\frac{1}{n_e(V)^2} = \frac{\cos^2(\theta(V))}{n^2{}_e} + \frac{\sin^2(\theta(V))}{n^2{}_0}. \tag{A5}$$

Using $n_e(V)$ and n_0, which remains constant, a Jones matrix is written for each layer. These matrices are then multiplied to obtain a single potential dependent matrix LC, which is dependent on the refractive indices, the wavelength of light, λ, the cell thickness, d_{LC}, and the cell twist angle in radians (here $\pi/2$):

$$LC = \begin{bmatrix} \cos(\gamma) - i\left(\frac{\beta}{\gamma}\right)\sin(\gamma) & \left(\frac{\pi}{2\gamma}\right)\sin(\gamma) \\ \left(\frac{\pi}{2\gamma}\right)\sin(\gamma) & \cos(\gamma) + i\left(\frac{\beta}{\gamma}\right)\sin(\gamma) \end{bmatrix}. \tag{A6}$$

The factors β and γ depend on the refractive indices and are

$$\beta(V) = \frac{\pi d_{\mathrm{LC}}}{\lambda}\left[n_e(V) - n_0\right], \tag{A7}$$

$$\gamma(V) = \sqrt{\pi^2 + \beta(V)}. \tag{A8}$$

For a 90° twisted nematic LC cell operated in the normally black mode (parallel polarizers) the substitution of the above nested equations, followed by the appropriate matrix multiplication [Eq. (A2)] and substitution [Eq. (A3)], gives LC cell transmission, T_{LC}, as a function of potential:

$$T_{\mathrm{LC}} = \frac{\pi}{2}\frac{\sin(\gamma(V))}{\gamma(V)}. \tag{A9}$$

[a]Electronic-mail: rowlands@srcl.sunnybrook.utoronto.ca

[1]A. D. A. Maidment, M. J. Yaffe, D. B. Plewes, G. E. Mawdsley, I. C. Soutar, and B. G. Starkoski, ''Imaging performance of a prototype scanned-slot digital mammography system,'' in *Physics of Medical Imaging*, edited by R. Shaw, Proc. SPIE **1896**, 93–103 (1993).

[2]A. Karellas, L. J. Harris, H. Liu, M. A. Davis, and C. J. D'Orsi, ''Charge coupled device detector: Performance considerations and potential for small-field mammographic imaging applications,'' Med. Phys. **19**, 1195–1199 (1992).

[3]L. E. Antonuk, J. Boudry, W. Huang, D. L. McShan, E. J. Morton, J. Yorkston, M. J. Longo, and R. A. Street, ''Demonstration of megavoltage and diagnostic x-ray imaging with hydrogenated amorphous silicon arrays,'' Med. Phys. **19**, 1455–1466 (1992).

[4]S. Hejazi and D. P. Trauernicht, ''System considerations in CCD-based x-ray imaging for digital chest radiography and digital mammography,'' Med. Phys. **24**, 287–298 (1997).

[5]A. Macovski, *Medical Imaging Systems* (Prentice-Hall, Toronto, 1983), pp. 81–82.

[6]J. Grinberg, A. Jacobson, W. Bleha, L. Miller, L. Fraas, D. Boswell, and G. Myer, ''A new real time noncoherent to coherent light image converter—The hybrid field effect liquid crystal light valve,'' Opt. Eng. (Bellingham) **14**, 217–225 (1975).
[7]D. Armitage, J. I. Thackara, and W. D. Eades, ''Photoaddressed liquid crystal spatial light modulators,'' Appl. Opt. **28**, 4763–4771 (1989).
[8]J.-P. Huignard, S. LeBerre, C. Mayeux, and F. Micheron, ''Liquid crystal image converter device,'' U. S. Patent 4 368 386, Jan. 11, 1983.
[9]P. Rieppo, B. Bahadur, and J. A. Rowlands, ''Amorphous selenium liquid crystal light valve for x-ray imaging,'' in *Physics of Medical Imaging*, edited by R. L. Van Metter and J. Beutel, Proc. SPIE **2432**, 228 (1995).
[10]J. W. Boag, ''Xeroradiography,'' Phys. Med. Biol. **18**, 3–37 (1973).
[11]U. Neitzel, I. Maack, and S. Guenther-Kohlfahl, ''Image quality of a digital chest radiography system based on a selenium detector,'' Med. Phys. **21**, 509–516 (1994).
[12]E. F. Plechaty, D. E. Cullen, and R. J. Howerton, *Tables and graphs of photon interaction cross sections from 1.0 keV to 100 MeV derived from LLL evaluated nuclear data library. UCRL-50400 Vol. 6 revision 1* (University of California Lawrence Livermore Laboratory, Springfield, VA, 1975; National Technical Information Service, 1975).
[13]H. Fiedler and F. Laugwitz, ''Zur Quantenausbeute elektroradiograpischer Selenschichten,'' J. Signal AM **9**, 229–235 (1981).
[14]J. A. Rowlands, G. DeCrescenzo, and N. Araj, ''X-ray imaging using amorphous selenium: Determination of x-ray sensitivity by pulse height spectroscopy,'' Med. Phys. **19**, 1065–1069 (1992).
[15]W. Que and J. A. Rowlands, ''X-Ray imaging using amorphous selenium: Inherent spatial resolution,'' Med. Phys. **22**, 365–374 (1995).
[16]R. K. Swank, ''Calculation of modulation transfer functions of x-ray fluorescent screens,'' Appl. Opt. **12**, 1865–1870 (1973).
[17]N. F. Mott and E. A. Davis, *Electronic Processes in Noncrystalline Materials* (Clarendon, Oxford, 1979), p. 531.
[18]B. Bahadur, ''Liquid crystal displays,'' in *Molecular Crystals and Liquid Crystals—Special Topics X*, edited by G. J. Dienes, M. M Labes, and G. H. Brown (Gordon and Breach, New York, 1984), pp. 81, 47–49.
[19]*Liquid Crystals—Applications and Uses*, Vol. 1, edited by B. Bahadur (World Scientific, New Jersey, 1990), pp. 239–240.
[20]*Liquid Crystal Mixtures For Electro-Optical Displays* (Merck Ltd./BDH Publication, Darmstadt, 1992).
[21]K. Lu and B. E. A. Saleh, ''Theory and design of the liquid crystal TV as an optical spatial phase modulator,'' Opt. Eng. (Bellingham) **29**, 240–246 (1990).
[22]F. A. Allan, ''The optimization of twisted nematic display thicknesses,'' in *Selected Papers on Liquid Crystals for Optics*, edited by S. D. Jacobs and B. J. Thompson (SPIE Optical Engineering Press, Bellingham, WA, 1992), pp. 224–225.
[23]D. M. Pai and R. C. Enck, ''Onsager mechanism of photogeneration in amorphous selenium,'' Phys. Rev. B **11**, 5163–5174 (1975).
[24]H. W. Ott, *Noise Reduction Techniques in Electronic Systems*, 2nd Ed. (Wiley, Toronto, 1988), pp. 228–243.
[25]R. M. Schaffert, *Electrophotography* (Focal, London, 1980), pp. 476–511, 93, 266.
[26]R. Birch, M. Marshall, and G. M. Ardran, *Catalogue of Spectral Data For Diagnostic X-rays*, *Scientific Report Series No. 30* (Hospital Physicists' Association, London, 1979).
[27]R. M. Nishikawa, G. E. Mawdsley, A. Fenster, and M. Yaffe, ''Scanned-projection digital mammography,'' Med. Phys. **14**, 717–727 (1987).
[28]M. M. Tesic, R. A. Mattson, G. T. Barnes, R. A. Sones, and J. B. Stickney, ''Digital radiography of the chest: Design features and considerations for a prototype unit,'' Radiology **148**, 259–264 (1983).
[29]H. E. Johns and J. R. Cunningham, *The Physics of Radiology* (Charles C. Thomas, Springfield, IL, 1983), p. 722.
[30]P. C. Bunch, ''Detective quantum efficiency of selected mammographic screen-film combinations,'' in *Medical Imaging III: Image Formation*, edited by R. H. Schneider, S. J. Dwyer III, and R. G. Jost, Proc. SPIE **1090**, 67–77 (1989).
[31]*MTFs and Wiener Spectra of Radiographic Screen-Film Systems, Volume II, HHS publication FDA 86-8257* (U.S. Department of Health and Human Services, Public Health Service, FDA, Rockville, MD, 1986), p. 81.
[32]J. T. Dobbins, D. L. Ergun, L. Rutz, D. A. Hinshaw, H. Blume, and D. C. Clark, ''DQE(f) of four generations of computed radiography acquisition devices,'' Med. Phys. **22**, 1581–1593 (1995).
[33]R. Fahrig, J. A. Rowlands, and M. Yaffe, ''X-ray imaging with amorphous selenium: Detective quantum efficiency of photoconductive receptors for digital mammography,'' Med. Phys. **22**, 153–160 (1995).
[34]C. Soutar and K. Lu, ''Determination of the physical properties of an arbitrary twisted-nematic liquid crystal cell,'' Opt. Eng. (Bellingham) **33**, 2704–2712 (1994).
[35]A. Yariv and P. Yeh, *Optical Waves in Crystals* (Wiley, New York, 1984), Chap. 5.